RSC Advances

PAPER

View Article Online
View Journal | View Issue

Cite this: *RSC Adv.*, 2017, **7**, 46713

A broad-band orange-yellow-emitting $Lu_2Mg_2Al_2Si_2O_{12}$: Ce^{3+} phosphor for application in warm white light-emitting diodes

Yunan Zhou,[a] Weidong Zhuang,*[a] Yunsheng Hu,*[a] Ronghui Liu,[a] Zhouqing Jiang,[a] Yuanhong Liu,[a] Yanfeng Li,[a] Yaling Zheng,[a] Lei Chen[a] and Jiyou Zhong[b]

Received 8th August 2017
Accepted 29th September 2017

DOI: 10.1039/c7ra08760h

rsc.li/rsc-advances

A new garnet-type $Lu_2Mg_2Al_2Si_2O_{12}$ compound was successfully synthesized *via* high-temperature solid–state reaction. The crystal structure was confirmed by the Rietveld refinement method and belongs to a cubic system with a space group of $Ia\bar{3}d$ (230) and cell parameters of $a = b = c = 11.88310(1)$ Å. There are two different crystallographic positions for Mg^{2+} with coordination numbers of eight and six, respectively. A relatively large band gap (4.83 eV) was estimated by the diffuse reflectance spectrum, indicating that $Lu_2Mg_2Al_2Si_2O_{12}$ may be a promising host matrix for luminescent materials. The synthetic Ce^{3+}-doped $Lu_2Mg_2Al_2Si_2O_{12}$ phosphor shows intense and broad-band orange-yellow emission peaking at about 575 nm under near-ultraviolet (n-UV) and blue light excitation. Additionally, the quantum efficiency, thermal stability, and packing performance were investigated to evaluate the practical use in white LEDs. The results indicate that $Lu_2Mg_2Al_2Si_2O_{12}$: Ce^{3+} may be a promising orange-yellow phosphor for warm white LEDs.

1. Introduction

White light-emitting diodes (w-LEDs) have recently received intensive attention because of their superior advantages, such as high efficiency, low power consumption, great stability, and eco-friendliness.[1–3] Combination of the yellow-emitting phosphor $Y_3Al_5O_{12}$: Ce^{3+} (YAG: Ce^{3+}) with a blue InGaN chip is considered to be one of the most common and efficient ways to generate w-LEDs.[4] However, this combination usually generates cool white light with a modest color-rendering index (CRI, R_a) of ~75 due to the lack of red emission.[5–8] Thus, there is a drive to develop new orange-yellow-emitting phosphors that show a broad-band emission with an intensified red component to obtain warm w-LEDs.[9,10]

As an important part of w-LEDs, phosphors are required to exhibit a high quantum efficiency and small thermal quenching. According to the work of Seshadri and co-workers, a large Debye temperature (Θ_D) could be a predictor of high quantum efficiency (QE), and a wide band gap (E_g) of host is necessary to limit thermal quenching.[11] Typically, the well-known yttrium aluminium garnet (YAG) matrix owns a large Debye temperature (726 K) and a wide band gap (6.43 eV); and correspondingly, YAG: Ce^{3+} phosphor shows a high QE (~90) and small thermal quenching.[11,12] Furthermore, Ce^{3+}-doped compositional derivatives of YAG with these outstanding characteristics have also been reported and lead to a wide variety of applications, such as the commercial green $Lu_3Al_5O_{12}$: Ce^{3+} and $Ca_3Sc_2Si_3O_{12}$: Ce^{3+} phosphors.[13,14] Therefore, it is preferable for many researchers to focus on the garnet structure when searching for new phosphor hosts.

Garnet structure belongs to the cubic system (space group of $Ia\bar{3}d$) with a general formula $\{C\}_3[A]_2(D)_3O_{12}$. Wherein, {C}, [A], and (D) represent the cations that occupy 24c, 16a, and 24d Wychoff positions and are surrounded by 8, 6, and 4 oxygen atoms to form dodecahedron, octahedron, and tetrahedron, respectively.[15–17] The solid solution design for the host compound through cation/anion substitution, cosubstitution, or chemical-unit substitution is well employed for the photoluminescence tuning.[18–20] Especially, garnet phosphors exhibit unique tunability of luminescence properties by chemical substitutions on the {C}, [A], and (D) cation sublattices.[21,22] On that basis, a large amount of Ce^{3+}-doped garnet hosts with various emission colors have been developed and reported, such as cyan $Ca_2LuHf_2(AlO_4)_3$: Ce^{3+} and $Ca_3Zr_2SiGa_2O_{12}$: Ce^{3+} phosphors, green $CaLu_2Al_4SiO_{12}$: Ce^{3+} and $Mg_{1.5}Lu_{1.5}Al_{3.5}Si_{1.5}O_{12}$: Ce^{3+} phosphors, yellow $Y_3Mg_xSi_xAl_{5-2x}O_{12}$: Ce^{3+} and $Lu_{3-x}Y_xMgAl_3SiO_{12}$: Ce^{3+} solid solution phosphors, and orange $Lu_2CaMg_2(Si,Ge)_3O_{12}$: Ce^{3+} phosphor.[23–29] It is worth noticing that Mg^{2+} can not only be incorporated into [A] sites, such as $Y_3Mg_xSi_xAl_{5-2x}O_{12}$: Ce^{3+}, but also be introduced in {C} sites, such as $Mg_{1.5}Lu_{1.5}Al_{3.5}Si_{1.5}O_{12}$: Ce^{3+}. However, Mg^{2+}–Si^{4+} incorporation into the [A] and (D) sites, respectively, leads to the

[a]National Engineering Research Center for Rare Earth Materials, General Research Institute for Nonferrous Metals, Grirem Advanced Materials Co., Ltd., Beijing 100088, PR China. E-mail: wdzhuang@126.com; hongyu1136@126.com
[b]School of Physics and Optoelectronic Engineering, Guangdong University of Technology, Guangzhou 510006, PR China

red shift of Ce^{3+} emission, but Mg^{2+}–Si^{4+} substitution on the {C} and (D) sites, respectively, can shift the Ce^{3+} emission to the short wavelength.[26,27] The above results indicate that Mg^{2+} incorporation into dodecahedral or octahedral sites has totally different effects on the coordination environment for Ce^{3+}. However, there is few research on the incorporation of Mg^{2+} into both {C} and [A] sites and its effect on luminescence properties.

Motivated by the above knowledge, we designed a new $Lu_2Mg_2Al_2Si_2O_{12}$ composition based on the typical $Lu_3Al_5O_{12}$ matrix, where a Lu^{3+} ({C} site) as well as an Al^{3+} ([A] site) are substituted by two Mg^{2+}, and for charge neutrality two other Al^{3+} ((D) site) are simultaneously replaced by two Si^{4+}. The Rietveld refinement results confirmed that Mg^{2+} ions were incorporated into both dodecahedral and octahedral sites as designed. And the luminescence properties of Ce^{3+}-doped $Lu_2Mg_2Al_2Si_2O_{12}$ were investigated systematically. The obtained $Lu_2Mg_2Al_2Si_2O_{12}$: Ce^{3+} phosphor shows intense orange-yellow emission containing more red component than that of YAG: Ce^{3+} under blue light excitation. Furthermore, the temperature-dependent photoluminescence behaviours as well as the fabrication properties of the phosphor were studied to evaluate the applicability as a color converter for w-LEDs.

2. Experimental

2.1. Materials and synthesis

Polycrystalline samples of $Lu_{2-x}Mg_2Al_2Si_2O_{12}$: xCe^{3+} ($x = 0$, 0.02, 0.04, 0.06, 0.08, 0.10, 0.12) were synthesized by high-temperature solid–state reaction. The starting materials (Lu_2O_3, 99.99%; MgO, 99.95%; Al_2O_3, 99.99%; SiO_2, 99.99%; CeO_2, 99.995%) were all weighed out in the desired stoichiometry and thoroughly mixed. The mixtures were put in an alumina crucible and continually fired at 1400 °C in a reducing atmosphere of H_2/N_2 (3/1) for 6 h. Then the samples were furnace-cooled continuously to room temperature, and ground well for the subsequent measurements. The commercial YAG: Ce^{3+} phosphor used for comparison was manufactured by Grirem Advanced Materials Co., Ltd. The blue InGaN chips ($\lambda_{ex} = 455$ nm) were purchased from Hang Zhou Silan Azure Co., Ltd.

2.2. Characterization methods

The phase structure determination of the as-prepared samples were carried out by a powder X-ray diffractometer (Rigaku, Japan) with Co-Kα radiation ($\lambda = 0.178752$ nm), and the date were recorded in the 2θ range of 10–80° with scan step of 6° min^{-1}. The XRD data, for structural refinement, of $Lu_{1.94}Mg_2Al_2Si_2O_{12}$: $0.06Ce^{3+}$ were collected on a powder X-ray diffractometer (PANalytical, Holland) with Cu-Kα radiation ($\lambda = 0.154056$ nm) in the 10–120° range (2θ) with scan speed of 0.0170° s^{-1}. Diffuse reflection (DR) spectra were detected on an UV-Vis-NIR spectrophotometer (SHIMADZU, Japan) with an integrated sphere attachment, and $BaSO_4$ powder sample served as a standard. The room-temperature photoluminescence (PL) and photoluminescence excitation (PLE) spectra, as well as the temperature-dependent photoluminescence properties, were measured by a Fluoromax-4 spectrofluorometer (Edison, USA) equipped with a 200 W xenon lamp, a photomultiplier tube operating, and a heating attachment. The fluorescent decay curves were measured on a TemPro-01 time-resolved fluorescence spectrofluorometer (Horbia Jobin Yvon, France). The quantum efficiency (QE) value was measured by an intensified multichannel QE-2100 spectrometer (Otsuka Electronics, Japan) equipped with a Xe lamp. The Commission International de I'Eclairage (CIE) chromaticity coordinates of samples were determined by a DT-101 colour analyser with a CCD detector (Laiko, Japan).

3. Results and discussion

3.1. Phase and crystal analysis

Fig. 1 presents the XRD patterns for the series of $Lu_{2-x}Mg_2Al_2Si_2O_{12}$: xCe^{3+} samples with different doped concentrations of Ce^{3+} ($x = 0$, 0.02, 0.04, 0.06, 0.08, 0.10, 0.12). The diffraction peaks of all these samples could be indexed to the $Ia\bar{3}d$ space group of the cubic system, and no diffraction peak of impurities was observed. It indicates that the single-phased $Lu_2Mg_2Al_2Si_2O_{12}$ compound can be attained by the given synthesis conditions and the dopant concentration of Ce^{3+} in the designated range didn't incur any impurities or cause significant structure change in the host. Moreover, the diffraction peaks slightly shift to the low-angle side with the increasing Ce^{3+} concentration (as shown in the right panel of Fig. 1), meaning the expansion of the lattice caused by the substitution of Lu^{3+} ($r^{VIII} = 97.7$ pm) by Ce^{3+} ($r^{VIII} = 114.3$ pm).[30]

To confirm the phase structure and obtain detailed crystallographic information of the as-prepared samples, Rietveld structural refinement of XRD patterns for the selected $Lu_{1.94}Mg_2Al_2Si_2O_{12}$: $0.06Ce^{3+}$ sample was performed (as shown in Fig. 2) by GSAS software package.[31,32] In the process, the single-crystal structure data of $Lu_3Al_5O_{12}$ (ICSD no. 23846) were used as an initial model. The refinement process was stably convergent to $\chi^2 = 6.30$, $R_{wp} = 4.04\%$, $R_p = 5.55\%$, which makes sure

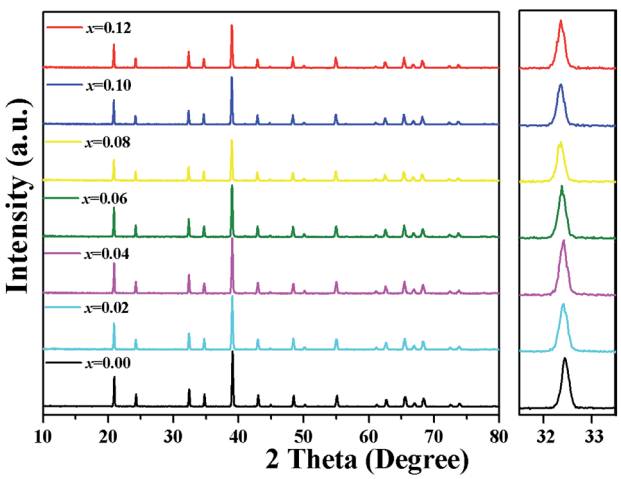

Fig. 1 XRD patterns of $Lu_{2-x}Mg_2Al_2Si_2O_{12}$: xCe^{3+} samples with different Ce^{3+} ($0 \le x \le 0.12$). Right panel: the magnified patterns in the 2-theta range of 31.5–33.5°.

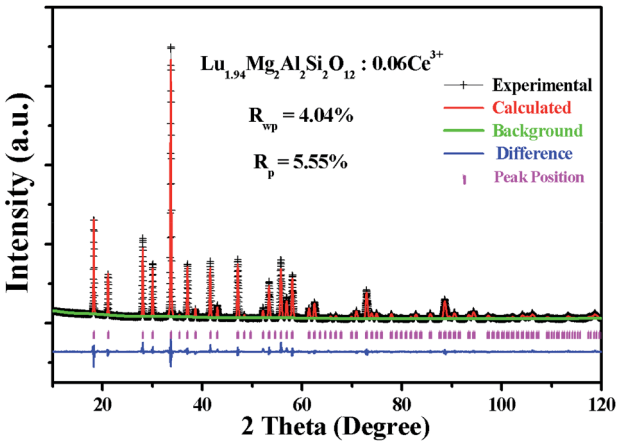

Fig. 2 Rietveld refinement XRD patterns of the selected $Lu_{1.94}Mg_2Al_2Si_2O_{12}$: $0.06Ce^{3+}$ sample.

the formation of a single garnet phase. The final refined structure data and residual factors are listed in Table 1. Wherein, the unit cell parameters were $a = b = c = 11.88310(1)$ Å and $V = 1677.991(3)$ Å^3.

From the refinement results, Fig. 3(a) displays a schematic diagram of the $Lu_{1.94}Mg_2Al_2Si_2O_{12}$: $0.06Ce^{3+}$ garnet structure. The dodecahedral, octahedral, and tetrahedral sites are randomly occupied by Lu/Mg/Ce (1.94/1/0.06), Mg/Al (1/1) and Al/Si (1/2), coordinated by eight, six and four oxygen ions, respectively. In addition, the [(Lu/Mg/Ce)O_8] dodecahedron connects with neighbour [(Mg/Al)O_6] octahedrons or other dodecahedrons by sharing edge, but connects with part of neighbour [(Al/Si)O_4] tetrahedrons by sharing edge and the other by sharing one O point, as shown in Fig. 3(b). Actually, each [(Lu/Mg/Ce)O_8] dodecahedron is surrounded by four [(Lu/Mg/Ce)O_8] dodecahedrons, four [(Mg/Al)O_6] octahedrons and six [(Al/Si)O_4] tetrahedrons, indicating that the photoluminescence of Ce^{3+} would be affected by the floating ratio of Lu/Mg/Ce, Mg/Al and Al/Si in surrounding dodecahedrons, octahedrons and tetrahedrons, respectively.

Table 1 Main results of Rietveld refinement of the $Lu_{1.94}Mg_2Al_2Si_2O_{12}$: $0.06Ce^{3+}$ sample

Crystal system					cubic
Space group					$Ia\bar{3}d$
$a = b = c$ (Å)					11.88310(1)
$\alpha = \beta = \gamma$ (deg)					90
V (Å^3)					1677.991(3)
Z					8
R_{wp} (%)					4.04
R_p (%)					5.55
χ^2					6.30
Atom	Site	Occu.	x	y	z
Lu	24c	0.6467	0.12500	0.000000	0.25000
Ce	24c	0.02000	0.12500	0.000000	0.25000
Mg_1	24c	0.3333	0.12500	0.000000	0.25000
Mg_2	16a	0.5000	0.00000	0.000000	0.00000
Al_1	16a	0.5000	0.00000	0.000000	0.00000
Al_2	24d	0.3333	0.37500	0.000000	0.25000
Si	24d	0.6667	0.37500	0.000000	0.25000
O	96h	1.0000	−0.03863	0.052202	0.15270

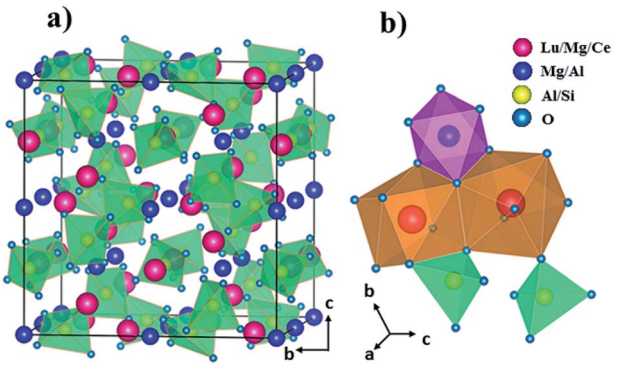

Fig. 3 (a) Structure of $Lu_{1.94}Mg_2Al_2Si_2O_{12}$: $0.06Ce^{3+}$ along *a* axis and (b) the connection between polyhedrons.

3.2. Photoluminescence properties

Fig. 4 depicts the diffuse reflectance (DR) spectra of the as-prepared $Lu_2Mg_2Al_2Si_2O_{12}$ host and $Lu_{1.92}Mg_2Al_2Si_2O_{12}$: $0.08Ce^{3+}$ phosphor. For the $Lu_2Mg_2Al_2Si_2O_{12}$ host, the DR spectrum shows an intense reflection in the visible range (380–780 nm), and a drastic decrease in the ultraviolet range (200–350 nm) originating from the valence-to-conduction transitions. The band gap value (E_g) of the $Lu_2Mg_2Al_2Si_2O_{12}$ host can be estimated by the following equation:[33,34]

$$[F(R_\infty)h\nu]^n = A(h\nu - E_g) \quad (1)$$

where $h\nu$ and A refer to the photon energy and a proportional constant, respectively; $R_\infty = R_{sample}/R_{standard}$; $n = 1/2$ for an

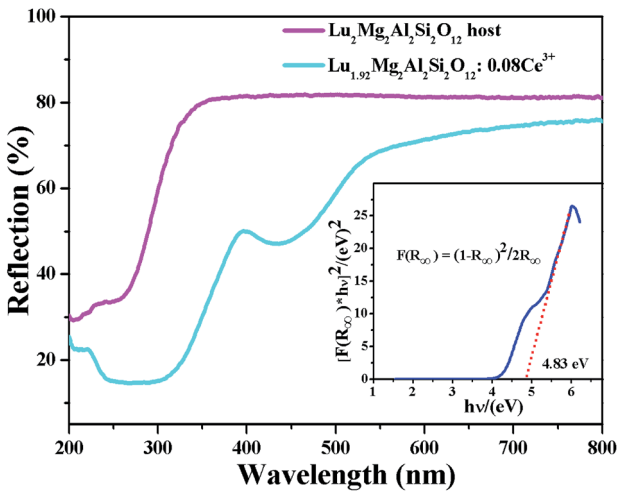

Fig. 4 Diffuse reflectance spectra of $Lu_2Mg_2Al_2Si_2O_{12}$ host and $Lu_{1.92}Mg_2Al_2Si_2O_{12}$: $0.08Ce^{3+}$ phosphor. Inset: the band gap calculation of $Lu_2Mg_2Al_2Si_2O_{12}$ host.

indirect transition or 2 for a direct transition; and $F(R_\infty)$ is the remission (Kubelka–Munk) function, defined as[35]

$$F(R\infty) = K/S = (1 - R_\infty)^2/2R_\infty \quad (2)$$

where K, and S represent the absorption and scattering coefficient, respectively. Through the linear extrapolation of $[F(R_\infty)h\nu]^n = 0$ (as shown in the inset of Fig. 4), the E_g value was determined to be about 4.83 eV. When 8 mol% of Ce^{3+} was doped into the $Lu_2Mg_2Al_2Si_2O_{12}$ host lattice, the DR spectrum exhibits enhanced absorption and two broad valleys (300–350 nm and 400–500 nm), which is attributable to the 4f–5d transitions of Ce^{3+} and consistent with the excitation spectrum.

Fig. 5 shows the room-temperature photoluminescence excitation (PLE) and emission (PL) spectra of $Lu_{1.92}Mg_2Al_2Si_2O_{12}$: $0.08Ce^{3+}$. The PLE spectrum (monitored at 575 nm), ranging from 300–540 nm, possesses a strong excitation band (about 370–540 nm) peaking at about 436 nm and a weak excitation band (about 300–360 nm) peaking at about 325 nm, corresponding to transitions of Ce^{3+} from the ground state (4f) to the two lowest excited levels ($5d_1$ and $5d_2$, respectively). As also shown in Fig. 5, the PL spectrum of $Lu_{1.92}Mg_2Al_2Si_2O_{12}$: $0.08Ce^{3+}$ under 436 nm excitation exhibits an asymmetric broad band (about 480–750 nm) peaking at 575 nm assigned to the 5d–4f transitions of Ce^{3+}.[36,37] The full width at half maximum (FWHM) of $Lu_{1.92}Mg_2Al_2Si_2O_{12}$: $0.08Ce^{3+}$ is calculated to be about 144 nm. Moreover, the asymmetric emission band can be resolved into two Gaussian profiles with peaks centered at 554 nm and 614 nm, respectively, which are attributed to the transitions from the lowest 5d excited state to the $^2F_{5/2}$ and $^2F_{7/2}$ ground states.[38,39] And the energy difference Δk between these two bands is about 1764 cm^{-1}, which is close to the theoretical energy difference between the $^2F_{5/2}$ and $^2F_{7/2}$ levels (~2000 cm^{-1}).[40,41]

In order to optimize the doping concentration of Ce^{3+} ion for this new garnet phosphor, the PL (λ_{ex} = 436 nm) spectra of $Lu_{2-x}Mg_2Al_2Si_2O_{12}$: xCe^{3+} samples with different concentrations of Ce^{3+} (x = 0.02, 0.04, 0.06, 0.08, 0.1, 0.12) were measured as shown in Fig. 6. The emission intensity increases with Ce^{3+} concentration increasing at first, reaches a maximum when x = 0.08, and then declines when Ce^{3+} concentration exceeds this critical concentration (also see the inset of Fig. 6) on account of concentration quenching effect.[42] The concentration quenching mainly results from non-radiative energy transfer among Ce^{3+} ions, whose occurring possibility increases as the content of Ce^{3+} increases. Three main mechanisms responsible for non-radiative energy transfer are exchange interaction, radiation reabsorption and multipolar interaction, respectively.[43,44] To make clear which mechanism dominates, it is requisite to obtain the critical distance (R_c) of energy transfer. The critical distance (R_c) among Ce^{3+} ions can be estimated based on the following formula:[45,46]

$$R_c = 2\left[\frac{3V}{4\pi x_c N}\right]^{\frac{1}{3}} \quad (3)$$

where V, x_c, and N refer to the unit cell volume, the critical concentration of activator, and the number of crystallographic sites in the unit cell that can be occupied by activator ions, respectively. In this case, the values V = 1677.991(28) Å^3, x_c = 0.08, and N = 24, and the obtained R_c value is 11.86. It's less likely that the exchange interaction mechanism plays the dominant role for the non-radiative energy transfer, because this mechanism generally requires a forbidden transition (the R_c value is ~5 Å).[47] Besides, the radiation reabsorption mechanism has an obvious effect only when there is a considerable overlap between the excitation and emission spectra. Thus, it is deduced that the electric multipolar interaction should take the main responsibility for non-radiative energy transfer between activator ions for $Lu_2Mg_2Al_2Si_2O_{12}$: Ce^{3+} phosphor.

Furthermore, the inset of Fig. 6 also depicts the dependence of peak wavelength on Ce^{3+} dopant concentration. It can be found that the peak wavelength of emission spectra gradually red-shifts from 561 nm for x = 0.02 to 580 nm for x = 0.12. The

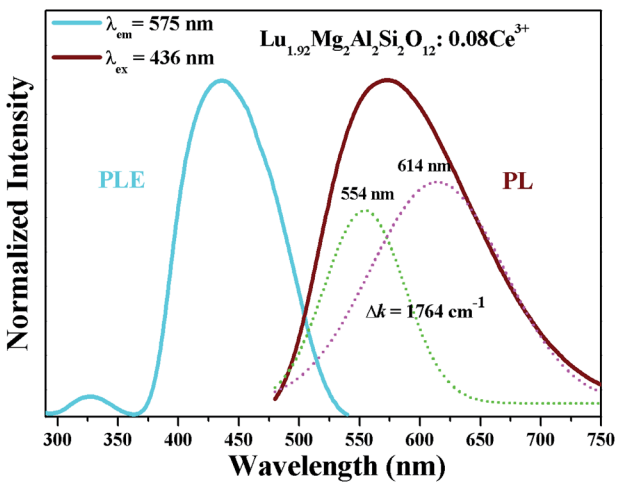

Fig. 5 PLE (λ_{em} = 575 nm) spectrum and PL (λ_{ex} = 436 nm) spectrum of $Lu_{1.92}Mg_2Al_2Si_2O_{12}$: $0.08Ce^{3+}$.

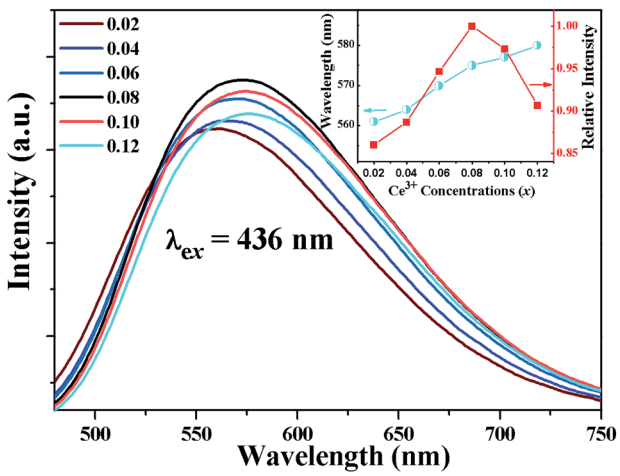

Fig. 6 PL spectra of $Lu_{2-x}Mg_2Al_2Si_2O_{12}$: xCe^{3+} ($0.02 \le x \le 0.12$). Insert: the dependence of emission intensity and peak wavelength on Ce^{3+} concentration.

redshift could be ascribed to the following two factors. First, the possibility of energy transfer from the Ce^{3+} ions at higher-energy sublevels of 5d to those at lower-energy sublevels increases with the increasing Ce^{3+} ion content, reducing the probability of the higher-energy emission. Second, as the substitution for smaller Lu^{3+} ions by larger Ce^{3+} ions increases, the crystal field strength surrounding Ce^{3+} ions enlarges, which causes a larger splitting of 5d levels and thus decreases the emission energy from the lowest excited level ($5d_1$) to the ground state (4f) of Ce^{3+}.[23] For these two factors, it is observed that the emission band of $Lu_2Mg_2Al_2Si_2O_{12}$: Ce^{3+} gradually red-shifts as the Ce^{3+} ion content increases.

Fig. 7 depicts the normalized PL spectra of the orange-yellow-emitting $Lu_{1.92}Mg_2Al_2Si_2O_{12}$: $0.08Ce^{3+}$ and the commercial yellow-emitting YAG: Ce^{3+} under 450 nm excitation. It is observed that the orange-yellow-emitting $Lu_{1.92}Mg_2Al_2Si_2O_{12}$: $0.08Ce^{3+}$ phosphor prepared by us contains more red-component emission than the commercial YAG: Ce^{3+} phosphor. In addition, the bandwidth of $Lu_{1.92}Mg_2Al_2Si_2O_{12}$: $0.08Ce^{3+}$ (FWHM = 144 nm) is wider than that of YAG: Ce^{3+} (FWHM = 124 nm). The results indicate that higher-quality white light obtained by coupling 455 nm blue InGaN chips with the orange-yellow-emitting $Lu_{1.92}Mg_2Al_2Si_2O_{12}$: $0.08Ce^{3+}$ phosphor is expected. In addition, the particularly broad emission band of $Lu_{1.92}Mg_2Al_2Si_2O_{12}$: $0.08Ce^{3+}$ phosphor may be due to the diverse local distortions of Ce^{3+}. Since the dodecahedral, octahedral and tetrahedral sites near Ce^{3+} ions are occupied by Lu^{3+}/Mg^{2+}, Mg^{2+}/Al^{3+} and Al^{3+}/Si^{4+}, respectively, the different distribution ratio of cation ions around Ce^{3+} results in the site-to-site variation of local crystalline environment and accordingly inhomogeneous broadening of the Ce^{3+} emission spectra.[48]

Fig. 8 shows the fluorescence decay curves of $Lu_{2-x}Mg_2Al_2Si_2O_{12}$: xCe^{3+} phosphors with varying Ce^{3+} contents (x = 0.02, 0.04, 0.06, 0.08, 0.1, 0.12) excited at 436 nm and monitored at 570 nm. It was found that these decay curves had parallel decay behaviours and all the curves can be fitted well by the mono-exponential function:[49]

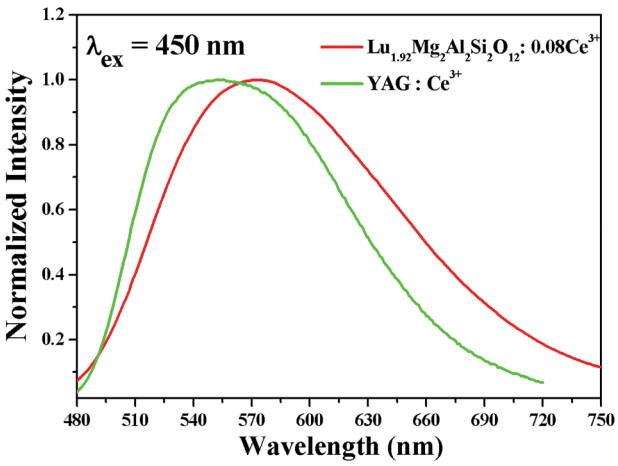

Fig. 7 Normalized PL spectra of $Lu_{1.92}Mg_2Al_2Si_2O_{12}$: $0.08Ce^{3+}$ and YAG: Ce^{3+}.

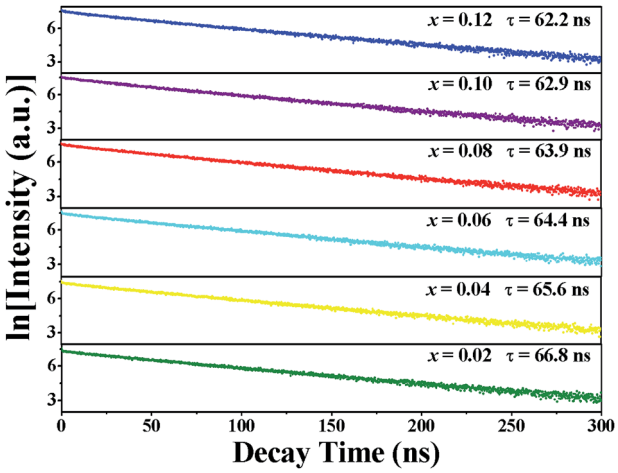

Fig. 8 Decay curves and calculated lifetime values of $Lu_{2-x}Mg_2Al_2Si_2O_{12}$: xCe^{3+} phosphors with different Ce^{3+} concentrations ($0.02 \leq x \leq 0.12$).

$$I(t) = A_1 \exp(-t/\tau) \quad (4)$$

where $I(t)$ and A_1 represent the photoluminescence intensity at time t and the initial intensity immediately after the exciting pulse, respectively, and t refers to fluorescence lifetime. And the decay times were determined by the fitting to be 66.8, 65.6, 64.4, 63.9, 62.9 and 62.2 ns for $Lu_{2-x}Mg_2Al_2Si_2O_{12}$: xCe^{3+} (x = 0.02, 0.04, 0.06, 0.08, 0.1, 0.12) phosphors, respectively. As Ce^{3+} concentration increases, both the possibility of energy transfer from Ce^{3+} ions to quenching sites and the energy transfer rate between Ce^{3+} ions increase, resulting in the decrease of the lifetime.[50] In addition, the well-fitting results by mono-exponential decay illustrate that Ce^{3+} ions only occupy one crystallographic site (24c) in the $Lu_2Mg_2Al_2Si_2O_{12}$ host in accordance with the Rietveld refinement result of $Lu_{1.94}Mg_2Al_2Si_2O_{12}$: $0.06Ce^{3+}$.

The temperature-dependent performance of phosphor is one of the significant technological parameters, which has a great effect on the luminous efficacy and color rendering performance of the w-LEDs, especially for phosphor-converted w-LEDs based on blue chips. The temperature-dependent emission spectra of $Lu_{1.92}Mg_2Al_2Si_2O_{12}$: $0.08Ce^{3+}$ phosphor under 436 nm excitation are presented in Fig. 8. As temperature rises from 25 to 200 °C, the emission intensity gradually declines due to the thermal quenching. All the spectral shape keeps similar with a weak blue shift (575 nm at 25 °C *vs.* 571 nm at 200 °C). The blue shift can be ascribed to the thermally activated phonon-assisted excitation from a lower-energy sublevel to a higher-energy sublevel of Ce^{3+} in the excited state.[51] The variation of emission intensity with temperature is also shown in the inset of Fig. 9. When the temperature reaches 150 °C, the emission intensity of $Lu_{1.92}Mg_2Al_2Si_2O_{12}$: $0.08Ce^{3+}$ phosphor drops to 74.9% of its initial intensity, indicating that this phosphor could exhibit excellent performance in the operation temperature range of w-LEDs. In case of the thermal quenching process only generated by the nonradiative relaxation process, the activation energy (barrier energy for thermal quenching) can be calculated by the Arrhenius equation:[52,53]

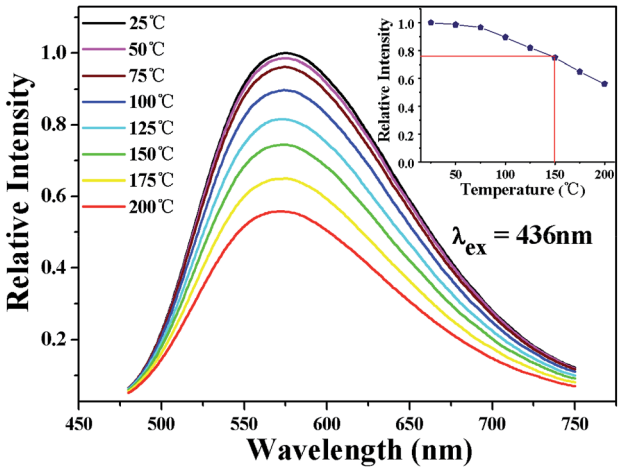

Fig. 9 Temperature-dependent PL (λ_{ex} = 436 nm) spectra of $Lu_{1.92}Mg_2Al_2Si_2O_{12}$: 0.08$Ce^{3+}$ phosphor. Insert: the relative emission intensity of $Lu_{1.92}Mg_2Al_2Si_2O_{12}$: 0.08$Ce^{3+}$ phosphor varying with temperature.

$$I_T = \frac{I_0}{1 + c\exp(-\Delta E/kT)} \quad (5)$$

where I_0 is the initial emission intensity; I_T represents the emission intensity at different testing temperatures; c is a constant; ΔE is the activation energy of thermal quenching; and k is the Boltzmann constant (8.629×10^{-5} eV K^{-1}). By linear fitting the relationship of $\ln[(I_0/I_T) - 1]$ *vs.* $1000/T$ with a slope of −4.075 got, the activation energy was calculated to be 0.351 eV (as shown in Fig. 10). The relatively high activation energy of this phosphor also illustrates its excellent thermal properties.

3.3. CIE chromaticity coordinates, quantum efficiency, and w-LED device performance

The CIE chromaticity coordinates of $Lu_{2-x}Mg_2Al_2Si_2O_{12}$: xCe^{3+} with different Ce^{3+} doped concentrations ($0.02 \leq x \leq 0.12$) under 436 nm excitation are depicted in Fig. 11. The color coordinates are shown as ranging from (0.458, 0.516) for x = 0.02 to (0.493, 0.493) for x = 0.12, which means that these phosphors may serve as orange-yellow-emitting phosphors for w-LEDs applications. Besides, the image of $Lu_{1.92}Mg_2Al_2Si_2O_{12}$: 0.08$Ce^{3+}$ phosphor under blue light radiating is also presented in the inset of Fig. 11, and intense orange-yellow light can be clearly caught by the naked eye. Furthermore, the internal and external QE of the optimal $Lu_{1.92}Mg_2Al_2Si_2O_{12}$: 0.08$Ce^{3+}$ phosphor under 436 nm excitation are measured to be about 72.6% and 53.3%, respectively. Generally, the QE value could be further improved by optimizing the preparation conditions.

The $Lu_2Mg_2Al_2Si_2O_{12}$: Ce^{3+} phosphor is great appropriate as a color converter for blue chip w-LEDs due to its strong blue light absorption and orange-yellow light emission. To further demonstrate the potential of $Lu_2Mg_2Al_2Si_2O_{12}$: Ce^{3+} phosphor for pc-wLEDs application, the $Lu_{1.92}Mg_2Al_2Si_2O_{12}$: 0.08$Ce^{3+}$

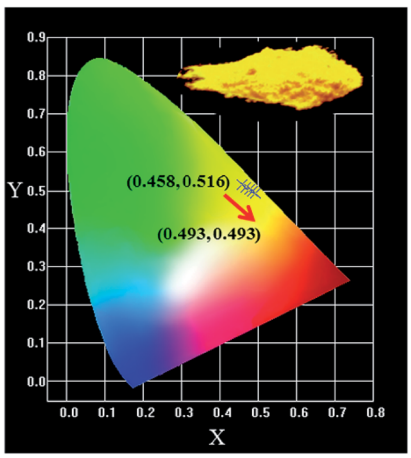

Fig. 11 The CIE coordinates of $Lu_{2-x}Mg_2Al_2Si_2O_{12}$: xCe^{3+} ($0.02 \leq x \leq 0.12$) and the image of $Lu_{1.92}Mg_2Al_2Si_2O_{12}$: 0.08$Ce^{3+}$ phosphor under blue light lamp.

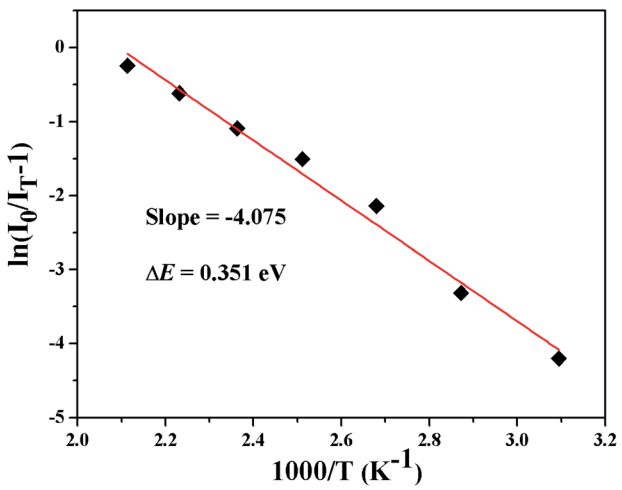

Fig. 10 Arrhenius fitting of the PL intensity of $Lu_{1.92}Mg_2Al_2Si_2O_{12}$: 0.08$Ce^{3+}$ phosphor as a function of temperature.

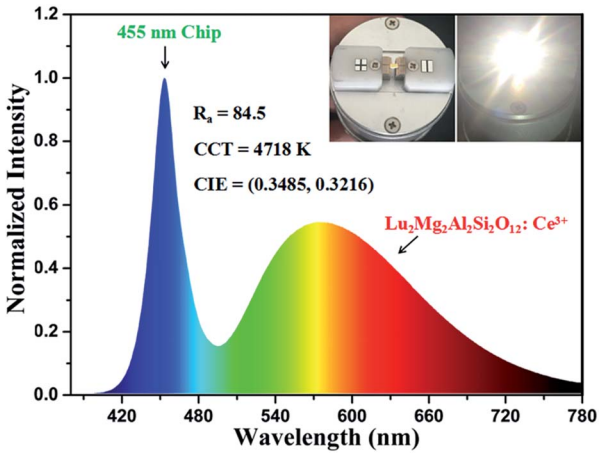

Fig. 12 Electroluminescence spectrum of a w-LED consisting of a blue InGaN chip and the $Lu_{1.92}Mg_2Al_2Si_2O_{12}$: 0.08$Ce^{3+}$ phosphor. Insert: as-prepared w-LED and w-LED in operation.

phosphor and a blue InGaN chip (λ_{ex} = 455 nm) were used to fabricate a w-LED device. Fig. 12 presents the electroluminescence (EL) spectrum of the as-fabricated w-LED device under 50 mA current operating. The device emits warm bright light with the CIE chromaticity coordinates of (0.3485, 0.3216) and relatively low correlated colour temperature (CCT) of 4718 K. And the colour rendering index (R_a) of this w-LED lamp was checked out to be 84.5, which is higher than that of the w-LEDs using blue chips pumped by YAG: Ce^{3+} phosphor (R_a = 75).[54] Consequently, $Lu_2Mg_2Al_2Si_2O_{12}$: Ce^{3+} displays significant potential as a w-LED phosphor, achieving high R_a and low CCT without blending additional red phosphor.

4. Conclusions

In summary, a new phosphor $Lu_2Mg_2Al_2Si_2O_{12}$: Ce^{3+} has been successfully synthesized *via* the high-temperature solid–state reaction method. Rietveld structural refinement results make sure the formation of a single garnet phase. Under excitation with n-UV to blue light, the $Lu_2Mg_2Al_2Si_2O_{12}$: Ce^{3+} phosphor exhibited intense broad-band orange-yellow emission (peaking at about 575 nm, FWHM = 144 nm) containing more red component than that of YAG: Ce^{3+}. The optimal dopant concentration of Ce^{3+} was x = 0.08, of which the internal quantum efficiency was about 72.6%. The corresponding concentration quenching mechanism is considered to be the electric multipolar interaction. When heated up to 150 °C, the $Lu_{1.92}Mg_2Al_2Si_2O_{12}$: $0.08Ce^{3+}$ phosphor still remained at about 75% of the emission intensity at room temperature. The w-LED device fabricated with a blue chip and the $Lu_2Mg_2Al_2Si_2O_{12}$: Ce^{3+} phosphor displayed the CIE color coordinate of (0.3485, 0.3216), CCT of 4718 K, and R_a value of 84.5. Those results indicate that $Lu_2Mg_2Al_2Si_2O_{12}$: Ce^{3+} may be a promising candidate for applications in n-UV and blue light excited warm white LEDs.

Conflicts of interest

There are no conflicts to declare.

Acknowledgements

This work was financially supported by the National Basic Research Program of China (2014CB643801).

References

1 S. Nakamura, T. Mukai and M. Senoh, *Appl. Phys. Lett.*, 1994, **64**, 1687–1689.
2 S. Pimputkar, J. S. Speck, S. P. DenBaars and S. Nakamura, *Nat. Photonics*, 2009, **3**, 180–182.
3 P. Pust, V. Weiler, C. Hecht, A. Tücks, A. S. Wochnik, A. K. Henß, D. Wiechert, C. Scheu, P. J. Schmidt and W. Schnick, *Nat. Mater.*, 2014, **13**, 891–896.
4 Y. Jia, R. Pang, H. Li, W. Sun, J. Fu, L. Jiang, S. Zhang, Q. Su, C. Li and R. S. Liu, *Dalton Trans.*, 2015, **44**, 11399–11407.
5 C. H. Huang and T. M. Chen, *Inorg. Chem.*, 2011, **50**, 5725–5730.
6 L. Y. Feng, Z. D. Hao, X. Zhang, L. L. Zhang, G. H. Pan, Y. S. Luo, L. G. Zhang, H. F. Zhao and J. H. Zhang, *Dalton Trans.*, 2016, **45**, 1539–1545.
7 F. Du, W. D. Zhuang, R. H. Liu, Y. H. Liu, J. Y. Zhong, W. Gao, K. Chen, L. Chen, K. Kato and K. Lin, *RSC Adv.*, 2016, **6**, 77059–77065.
8 N. Guo, H. P. You, Y. H. Song, M. Yang, K. Liu, Y. H. Zheng, Y. J. Huang and H. J. Zhang, *J. Mater. Chem.*, 2010, **20**, 9061–9067.
9 W. Z. Sun, Y. L. Jia, R. Pang, H. F. Li, T. F. Ma, D. Li, J. P. Fu, S. Zhang, L. H. Jiang and C. Y. Li, *ACS Appl. Mater. Interfaces*, 2015, **7**, 25219–25226.
10 L. L. Zhang, J. H. Zhang, X. Zhang, Z. D. Hao, H. F. Zhao and Y. S. Luo, *ACS Appl. Mater. Interfaces*, 2013, **5**, 12839–12846.
11 J. Brgoch, S. P. DenBaars and R. Seshadri, *J. Phys. Chem. C*, 2013, **117**, 17955–17959.
12 V. Bachmann, C. Ronda and A. Meijerink, *Chem. Mater.*, 2009, **21**, 2077–2084.
13 A. A. Setlur and A. Srivastava, *Opt. Mater.*, 2007, **29**, 1647–1652.
14 Y. Shimomura, T. Honma, M. Shigeiwa, T. Akai, K. Okamoto and N. Kijima, *J. Electrochem. Soc.*, 2007, **154**, J35–J38.
15 Y. R. Shi, G. Zhu, M. Mikami, Y. Shimomura and Y. H. Wang, *Dalton Trans.*, 2015, **44**, 1775–1781.
16 X. H. Gong, J. H. Huang, Y. J. Chen, Y. F. Lin, Z. D. Luo and Y. D. Huang, *Inorg. Chem.*, 2014, **53**, 6607–6614.
17 S. K. Hussain and J. S. Yu, *RSC Adv.*, 2017, **7**, 13281–13288.
18 M. M. Shang, S. S. Liang, N. R. Qu, H. Z. Lian and J. Lin, *Chem. Mater.*, 2017, **29**, 1813–1829.
19 Z. G. Xia and K. R. Poeppelmeier, *Acc. Chem. Res.*, 2017, **50**, 1222–1230.
20 Z. G. Xia, C. G. Ma, M. S. Molokeev, Q. L. Liu, K. Rickert and K. R. Poeppelmeier, *J. Am. Chem. Soc.*, 2015, **137**, 12494–12497.
21 Z. G. Xia and A. Meijerink, *Chem. Soc. Rev.*, 2017, **46**, 275–299.
22 Z. G. Xia and Q. L. Liu, *Prog. Mater. Sci.*, 2016, **84**, 59–117.
23 X. C. Wang, Z. Y. Zhao, Q. S. Wu, Y. Y. Li and Y. H. Wang, *J. Mater. Chem. C*, 2016, **4**, 11396–11403.
24 J. Y. Zhong, W. D. Zhuang, X. R. Xing, R. H. Liu, Y. F. Li, Y. L. Zheng, Y. S. Hu and H. B. Xu, *RSC Adv.*, 2015, **6**, 2155–2161.
25 A. Katelnikovas, J. Plewa, D. Dutczak, S. Möller, D. Enseling, H. Winkler, A. Kareiva and T. Jüstel, *Opt. Mater.*, 2012, **34**, 1195–1201.
26 Y. C. Jia, Y. J. Huang, N. Guo, H. Qiao, Y. H. Zheng, W. Z. Lv, Q. Zhao and H. P. You, *RSC Adv.*, 2012, **2**, 2678–2681.
27 M. M. Shang, J. Fan, H. Z. Lian, Y. Zhang, D. L. Geng and J. Lin, *Inorg. Chem.*, 2014, **53**, 7748–7755.
28 H. P. Ji, L. Wang, M. S. Molokeev, N. Hirosaki, Z. H. Huang, Z. G. Xia, O. M. ten Kate, L. H. Liu and R. J. Xie, *J. Mater. Chem. C*, 2016, **4**, 2359–2366.
29 A. A. Setlur, W. J. Heward, Y. Gao, A. M. Srivastava, R. G. Chandran and M. V. Shankar, *Chem. Mater.*, 2006, **18**, 3314–3322.

30 R. D. Shannon and C. T. Prewitt, *Acta Crystallogr.*, 1969, **25**, 925–946.
31 H. M. Rietveld, *J. Appl. Crystallogr.*, 1969, **2**, 65–71.
32 B. H. Toby, *J. Appl. Crystallogr.*, 2001, **34**, 210–213.
33 A. E. Morales, E. S. Mora and U. Pal, *Rev. Mex. Fis. S*, 2007, **53**, 18–22.
34 Y. J. Hua, X. J. Li, D. W. Zhang, H. P. Ma, D. G. Deng and S. Q. Xu, *New J. Chem.*, 2016, **40**, 5458–5466.
35 Z. J. Zhang, O. M. ten Kate, A. C. A. Delsing, Z. Y. Man, R. J. Xie, Y. F. Shen, M. J. H. Stevens, P. H. L. Notten, P. Dorenbos, J. T. Zhao and H. T. Hintzen, *J. Mater. Chem. C*, 2013, **1**, 7856–7865.
36 X. Ding, G. Zhu, W. Y. Geng, Q. Wang and Y. H. Wang, *CrystEngComm*, 2015, **17**, 3235–3242.
37 Y. L. Zheng, W. D. Zhuang, X. R. Xing, J. Y. Zhong, R. H. Liu, Y. F. Li, Y. H. Liu and Y. S. Hu, *RSC Adv.*, 2016, **6**, 68852–68859.
38 W.-R. Liu, C.-H. Huang, C.-P. Wu, Y.-C. Chiu, Y.-T. Yeh and T.-M. Chen, *J. Mater. Chem.*, 2011, **21**, 6869–6874.
39 R. J. Yu, S. L. Zhong, N. Xue, H. J. Li and H. L. Ma, *Dalton Trans.*, 2014, **43**, 10969–10976.
40 G. Blasse and B. C. Grabmaier, *Luminescent Materials*, Springer, Berlin, German, 1994, p. 45.
41 Y. Q. Li, N. Hirosaki, R. J. Xie, T. Takeda and M. Mitomo, *Chem. Mater.*, 2008, **20**, 6704–6714.
42 W. B. Im, S. Brinkley, J. Hu, A. Mikhailovsky, S. P. DenBaars and R. Seshadri, *Chem. Mater.*, 2010, **22**, 2842–2849.
43 S.-P. Lee, T.-S. Chan and T.-M. Chen, *ACS Appl. Mater. Interfaces*, 2015, **7**, 40–44.
44 J. Y. Zhong, W. D. Zhuang, X. R. Xing, R. H. Liu, Y. F. Li, Y. H. Liu and Y. S. Hu, *J. Phys. Chem. C*, 2015, **119**, 5562–5569.
45 G. Blasse, *Phys. Lett. A*, 1968, **28**, 444–445.
46 G. Blasse, *Philips Res. Rep.*, 1969, **24**, 131.
47 Z. W. Zhang, L. J. Wang, S. S. Yang, W. G. Chen and X. J. Chu, *Dyes Pigm.*, 2017, **142**, 272–276.
48 N. M. Khaidukov, V. N. Makhov, Q. H. Zhang, R. Shi and H. B. Liang, *Dyes Pigm.*, 2017, **142**, 524–529.
49 X. Chen, Z. G. Xia and Q. L. Liu, *Dalton Trans.*, 2014, **43**, 13370–13376.
50 S.-P. Lee, C.-H. Huang, T.-S. Chan and T.-M. Chen, *ACS Appl. Mater. Interfaces*, 2014, **6**, 7260–7267.
51 Z. G. Xia, X. M. Wang, Y. X. Wang, L. B. Liao and X. P. Jing, *Inorg. Chem.*, 2011, **50**, 10134–10142.
52 L. Chen, R. H. Liu, W. D. Zhuang, Y. H. Liu, Y. S. Hu, X. F. Zhou, W. Gao and X. L. Ma, *CrystEngComm*, 2015, **17**, 3687–3694.
53 G. Li, Y. Fan, H. J. Guo and Y. H. Wang, *New J. Chem.*, 2017, **41**, 5565–5571.
54 N. Komuro, M. Mikami, Y. Shimomura, E. G. Bithell and A. K. Cheetham, *J. Mater. Chem. C*, 2014, **2**, 6084–6089.